A coupled SPH DEM approach to model the interactions between multiple red blood cells in motion in capillary

Hasitha Nayanajith Polwaththe Gallage[a], Suvash C. Saha[a], Emilie Sauret[a], Robert Flower[b] and Y.T. Gu[a],*

[a] *School of Chemistry, Physics and Mechanical Engineering*
Queensland University of Technology, Brisbane, QLD 4001, Australia
[b] *Research Program Leader, Research and Development,*
Australian Red Cross Blood Service, Kelvin Grove, QLD 4059, Australia
* Corresponding author +61 7 3138 1009, yuantong.gu@qut.edu.au

Abstract

Red blood cells (RBCs) are the most common type of blood cells in the blood and 99% of the blood cells are RBCs. During the circulation of blood in the cardiovascular network, RBCs squeeze through the tiny blood vessels (capillaries). They exhibit various types of motions and deformed shapes, when flowing through these capillaries with diameters varying between 5-10 μm. RBCs occupy about 45 % of the whole blood volume and the interaction between the RBCs directly influences on the motion and the deformation of the RBCs. However, most of the previous numerical studies have explored the motion and deformation of a single RBC when the interaction between RBCs has been neglected. In this study, motion and deformation of two 2D (two-dimensional) RBCs in capillaries are comprehensively explored using a coupled smoothed particle hydrodynamics (SPH) and discrete element method (DEM) model. In order to clearly model the interactions between RBCs, only two RBCs are considered in this study even though blood with RBCs is continuously flowing through the blood vessels. A spring network based on the DEM is employed to model the viscoelastic membrane of the RBC while the inside and outside fluid of RBC is modelled by SPH. The effect of the initial distance between two RBCs, membrane bending stiffness (K_b) of one RBC and undeformed diameter of one RBC on the motion and deformation of both RBCs in a uniform capillary is studied. Finally, the deformation behavior of two RBCs in a stenosed capillary is also examined. Simulation results reveal that the interaction between RBCs has significant influence on their motion and deformation.

Keywords: Multiple Red blood cells, smoothed particle hydrodynamics, computational biomechanics, blood flow, meshfree method, hydrodynamics interactions

1. Introduction

Blood is a suspension of different blood cells in plasma and the majority of the blood cells are RBCs. The diameter of average healthy matured RBC varies between 6-8 μm (Dupire et al. 2012) at rest. The volumetric ratio of the RBCs to the total blood volume is called hematocrit and its value for a healthy person varies from 40 % to 50 % (Shvartsman,Fine 2003). The hematocrit value of the blood affects the motion and deformation of the RBCs as the interaction between RBCs makes a significant impact on the flow field. Fahraeus (1931) reported that the average volume fraction of the RBCs in the blood flow decreases when the capillary diameter decreases below 300 μm (Pozrikidis 2005; Secomb 1987). As a result, the discharge hematocrit (overall volumetric ratio of RBCs) is greater than the tube hematocrit (volumetric ratio of RBCs inside the capillary) which is known as Fahraeus effect. It has been found that the mechanical interaction between RBCs and capillary walls generally result in the formation of plasma layer, which leads to the Fahraeus effect (Pries et al. 1996; Bayliss 1959). However, very few studies are reported related to the motion and deformation of multiple RBCs and the influence of the interactions between the RBCs on their behavior. Furthermore, most of the studies have considered an average value for the diameter of the RBC and they have ignored the effects of the RBCs with different diameters on their motion and deformation behavior.

The effects of hematocrit value on the blood flow properties are investigated by Tsubota et. al (2006) using moving particle semi-implicit (MPS) method. However, they did not report how the motion or deformation of the RBCs changes when a RBC is infected by a disease such as malaria (Jiang et al. 2013). It is generally known that the motion and the deformation of the RBCs are significantly changed when they are infected by these diseases. Furthermore, most of the simulations were carried out for the RBCs in uniform capillaries previously without considering stenosed conditions in the capillaries. However, capillaries always do not have uniform cross sections and some of the capillaries have stenosed sections, where the cross sectional area of the capillary suddenly reduces. There is a high risk of micro vascular blockages in these areas (Cooke et al. 2001). Therefore, it is important to study the motion and deformation of the RBCs in the capillaries with these stenosed sections. Sun and Munn (2005) employed the Lattice Boltzmann approach to simulate the blood flow in blood

vessels. They reproduced the motion of blood cells in plasma to explain the experimental results, such as Fahraeus effect (Sun,Munn 2005). However, in their model the deformability nature of the RBCs were overlooked, since all the blood cells were modelled as rigid bodies (Tsubota et al. 2006). Pozrikidis (2005) revealed that the initial cell spacing or the tube hematocrit for a fixed capillary diameter influences the mean flow velocity and the deformation of the RBCs. However, their study did not focus closely on the effect of the mean velocity of the flow and deformation behavior of the RBCs when the properties of a specific RBC are changed due to the infection by a disease.

A three-dimensional model was developed by Nagayama and Honda (2012) to simulate the behavior of the RBCs in the capillary blood flow using moving particle semi implicit (MPS) method. In this method, instead of solving the Navier Stokes equations, a momentum equation for the RBC was developed, considering the inter-particle force, viscous diffusion and external force. They studied the motion and deformation of multiple RBCs in bent capillaries. However, a comprehensive analysis of the RBC behaviour in microchannels was not done by this model. Recently, dissipative particle dynamics (DPD) is employed to simulate the deformation and aggregation of healthy and infected RBCs in a capillary (Ye et al. 2014). However, the comprehensive investigation of the influence of interactions between RBCs on the motion and deformation in capillaries was not explained by this model.

The main objective of this study is to analyze the influence of the interactions between two RBCs on their motion and deformation. Specifically, this study aimed to investigate the effect of one RBC's properties on the motion and deformation of the other RBC due to the hydrodynamic interaction between them. In this study, coupled smoothed particle hydrodynamics (SPH), discrete element method (DEM) is used to analyze the influence of the interactions between two RBCs on their motion and deformation. The RBC membrane is modeled by a two dimensional spring network using fundamentals of DEM and the forces acting on the RBC membrane are determined based on the minimum energy concepts (Tsubota et al. 2006; Pan,Wang 2009; Polwaththe-Gallage et al. 2012). First, we present the motion and deformation of two RBCs in a uniform capillary. Next, we investigate the effect of the initial distance between two RBCs on the deformation behavior of the RBCs and how significant it is. Then, the effect of the membrane

bending stiffness (K_b) of one RBC on the motion and deformation of both RBCs in a uniform capillary is explored. Specifically, this study aims to predict the motion and deformation of two RBCs, when one RBC is having an uncharacteristic membrane bending stiffness due to the infection by a disease like malaria. Furthermore, we explore how the motion and deformation behavior of two RBCs change, when the initial diameter of one RBC changes, because of the average diameter of a healthy matured RBC varies between 6-8 μm. Moreover, the deformation behavior of two RBCs in abnormal blood vessels such as stenosis capillaries is investigated, where a micro vascular blockage could be happened. Finally, the effect of their interactions on motion and deformation behavior of both RBCs is explained. The main purpose of this study is to predict the effects of influence of the interactions between two red blood cells on motion and deformation under different pathological conditions. With the aid of this model the behavior of the RBCs predicted, particularly the details related to the blood flow rate can be projected, under the pathological conditions.

2. Model and methodologies

2.1 Two-dimensional RBC model

The membrane of the RBC is modelled by a two dimensional spring network (Polwaththe-Gallage et al. 2014). The RBC membrane is initially assumed to be a circle with the radius of 2.8 μm (Polwaththe-Gallage et al. 2014). Then it is discretized into 88 mass points and 88 springs are used to interconnect the neighboring mass points. In order to obtain a stable RBC membrane shape the total energy of the RBC membrane is considered. The total elastic energy stored in the springs due to stretching/compression (E_l) and bending (E_b) are calculated by

$$E_l = \frac{1}{2} K_l \sum_{i=1}^{N} \left(\frac{l_i - l_0}{l_o} \right)^2 \tag{1}$$

and

$$E_b = \frac{1}{2} K_b \sum_{i=1}^{N} \mathbf{tan}^2 \left(\frac{\theta_i}{2} \right) \tag{2}$$

where l_i, l_0, θ_i, K_l, and K_b are the present length of the ith spring, the original length of the same spring, the angle between two consecutive springs, the spring

constants for stretching/compression and the spring constants for bending respectively. Here, N is the number of springs, which are used to model the RBC membrane. In addition to the above elastic energies in **Eq**. **(1)** and **(2)**, an energy penalty function Es [**Eq**. **(3)**] is used to maintain a constant equivalent RBC membrane area(Polwaththe-Gallage et al. 2014) .

$$Es = \frac{1}{2} K_s \left(\frac{s - s_e}{s_e} \right)^2 \tag{3}$$

where s, s_e and K_s are the present cross sectional area, equivalent RBC membrane area and the penalty coefficient. The forces acting on the i^{th} membrane particle are calculated, using the principal of virtual work as in **Eq. (4)**:

$$\mathbf{F}_i = -\frac{\partial E}{\partial \mathbf{r}_i} \tag{4}$$

where the $\mathbf{r}_i$ is the position vector of the i^{th} membrane particle and the $\mathbf{F}_i$ is the vectorial force acting on the i^{th} membrane particle. The typical biconcave shape of the RBC with the radius of 7.64 μm and the thickness of 2.12 μm is obtained, when the total energy of the RBC membrane is minimized. This biconcave shape represents the morphology of an average healthy matured RBC. However, the biconcave shape of the RBC changes and exhibits more spherical shape, when the RBCs are infected by diseases such as malaria (Suresh et al. 2005). In this study, we use the obtained biconcave shape to represent the membrane of a healthy RBC. Therefore, the motion and deformation of the RBCs in capillaries is modelled with the aid of obtained biconcave shape.

2.1 SPH methodology

The inside and outside of the RBC membrane is discretized into a finite number of particles, to represent hemoglobin and plasma respectively. All the particles are treated by SPH method (Polwaththe-Gallage et al. 2014; Liu,Liu 2003; Morris et al. 1997). Navier-Stokes equation for the conservation of mass in Lagrangian form **[Eq. (5)]** is used calculate the forces acting on the SPH particles

$$\frac{D\mathbf{v}_i}{Dt} = -\sum_{j=1}^{N} m_j \left(\frac{p_j}{\rho_j^{\,2}} + \frac{p_i}{\rho_i^{\,2}} \right) \cdot \nabla_i W_{ij} + \sum_{j=1}^{N} m_j \frac{m_j \left(\mu_j + \mu_i\right)\left(\mathbf{r}_i - \mathbf{r}_j\right) \cdot \nabla_i W_{ij}}{\rho_j \rho_i \left|\mathbf{r}_i - \mathbf{r}_j\right|^2} \left(\mathbf{v}_i - \mathbf{v}_j\right) + \mathbf{f}_i \tag{5}$$

Where, **v**, p, ρ, μ, **r** and m are velocity, pressure, density, dynamic viscosity, position vector and mass of the SPH particles respectively, while i is the particle on focus and j is the neighboring particle (Liu,Liu 2003). Here, W is the smoothing kernel and in this study cubic spline smoothing function [**Eq. (6)]** is used.

$$W(R,h) = \frac{15}{7\pi h^2} \times \begin{cases} \frac{2}{3} - R^2 + \frac{1}{2}R^3 & \text{if } 0 \le R \le 1 \\ \frac{1}{6}(2-R)^3 & \text{if } 1 \le R \le 2 \\ 0 & \text{if } \quad R \ge 2 \end{cases} \tag{6}$$

where, $R = \left|\mathbf{r}_i - \mathbf{r}_j\right|/h$ and h is the smoothing length, which is set to 1.2 times the particle spacing, in order to improve the accuracy of the simulations (Liu,Liu 2003).

In the SPH method, theoretically incompressible fluids are considered as a slightly compressible fluid (Liu,Liu 2003). Artificial compression is introduced to the system to produce a pressure disturbance via quasi-incompressible equation of state [**Eq. (7**)]:

$$p = B\left(\left(\frac{\rho}{\rho_0} \right)^{\gamma} - 1 \right) \tag{7}$$

where B is a problem dependent parameter, in this study it is set to the initial pressure (Liu,Liu 2003), ρ_0 and ρ are initial and present density of the fluid particles respectively. Here γ is a constant and usually it is taken as $\gamma = 7$. This ensures large pressure variation correspond to the variations in density, which maintains the density variation less than 1% within the system.

Lenard Jones type repulsive forces [**Eq. (8)**] are applied to the fluid particles to avoid the penetration of fluid particles through solid membrane of the RBC (Polwaththe-Gallage et al. 2014).

$$\mathbf{F}_i = \begin{cases} D\left[\left(\dfrac{r_0}{r_i - r_j}\right)^{12} - \left(\dfrac{r_0}{r_i - r_j}\right)^{4}\right]\dfrac{(\mathbf{r}_i - \mathbf{r}_j)}{(r_i - r_j)^2} & \text{if } \left(\dfrac{r_0}{r_i - r_j}\right) \geq 1 \\ 0 & \text{if } \left(\dfrac{r_0}{r_i - r_j}\right) \leq 1 \end{cases} \tag{8}$$

where D is a problem dependent parameter, usually is equal to the square of the maximum velocity and r_0 is usually selected approximately close to the initial particle spacing (Liu,Liu 2003).

The Leap-Frog (LF) algorithm (Liu,Liu 2003) is used in time integration technique, due to its low memory storage requirement and high computational efficiency and the time step for following simulations is et to 1×10^{-9} s

3. Simulation results and discussion

The model considered here is validated against the simulation results published by Kaoui et al.(2011). They have established the steady state inclination angle for different area ratio (s*) values in RBC, when the RBC is subjected to a shear flow. Steady state of the RBC is observed when its morphology and the location almost do not change with time. The biconcave shape of the RBC is altered, by changing the equivalent area (s_e) of the RBC membrane. The area ratio (s*) is equal to s_e / s. When the area ratio is increased, the RBC membrane gives more circular shape. Four shapes with different area ratio values (s* = 0.6, 0.7, 0.8 and 0.9) are used for the purpose of validation and the relevant RBC membrane shapes are obtained (see **Fig 1**). In order to generate the shear flow, a constant velocity of 2×10^{-3} m/s is applied to the upper and lower walls of the flow channel (Polwaththe-Gallage et al. 2015).

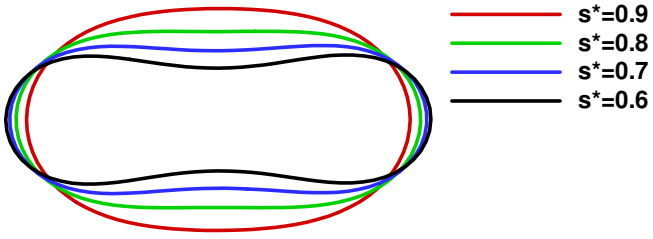

Fig 1 Equilibrium RBC shapes for different area ratios

The behavior of the four RBCs in a simple shear flow is examined. The time step is set to 10^{-9} s. The dynamic viscosity (μ) of hemoglobin, plasma and RBC particles is set to 10^{3} Pa.s and other simulation parameters are given in **Table 1**.

Table 1: Simulation Parameters

Parameter	Definition	Value	Reference
k_l	Spring constant for stretching/compression energy	5×10^{-8} Nm	(Pan,Wang 2009)
k_b	Spring constant for bending energy	5×10^{-10} Nm	(Pan,Wang 2009)
k_s	Penalty function constant	10^{-5} Nm	(Shi et al. 2012)
ρ_{rbc}	Density of RBC membrane	1098 kg/m^3	(Sun,Munn 2005)
ρ_{plasma}	Density of plasma	1025 kg/m^3	(Frcitas 1998)
$\rho_{cytoplasm}$	Density of cytoplasm	1050 kg/m^3	(Le et al. 2009)

The equilibrium inclination angles for four RBCs are measured and compared with the previously published results (Kaoui et al. 2011). The simulation results show a good agreement with previous results with less than 5% difference (see **Fig 2**).

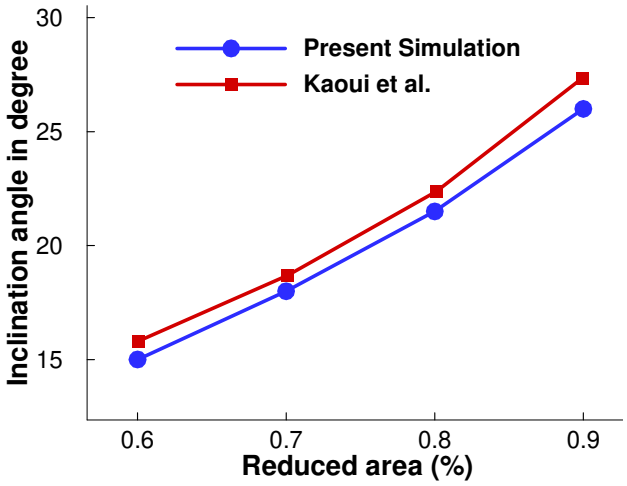

Fig 2 Equilibrium inclination angle of RBC for different area ratios

3.1 Motion and deformation of two RBCs in a uniform capillary

Motion and deformation of multiple RBCs in a uniform capillary is studied. The behavior of two RBCs in a uniform capillary is compared with the behavior of a single RBC in the same capillary (see **Fig 3**). The total length (L) and the diameter (D) of the capillary are set to 50 μm and 9.6 μm respectively. The inlet pressure is set to 512.5 Pa, while the outlet pressure is set to zero. In order to generate a flow in x-direction, the pressure exerted on the plasma particles located next to the inlet boundary is then converted into the body forces and applied on them. Thereby flow in x^+-direction is generated and the outflow through the inlet boundary (x^--direction) is avoided. Periodic boundary conditions are applied to the problem domain, such that any particle leaves the problem domain through the outlet boundary, immediately reenters the problem domain through the inlet boundary. No slip boundary conditions are applied to the top and bottom walls of the capillary.

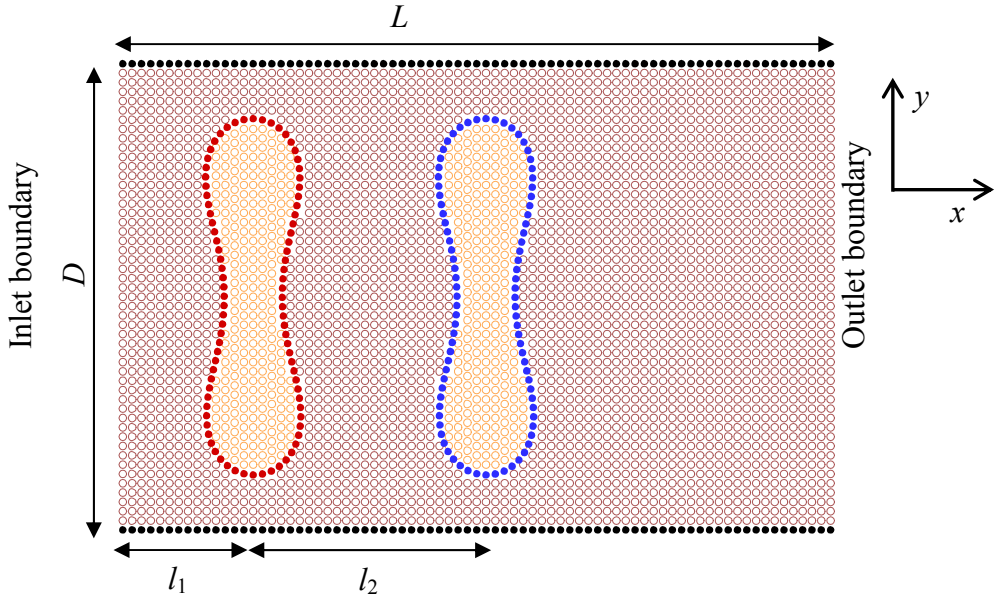

Fig 3: Initial particle configuration of the flow field with two RBCs

Due to the pressure gradient imposed into the capillary, plasma particles and RBCs start to move. For convenience, the right-side cell is defined as the leading RBC (1st RBC) and the left-side RBC is defined as the trailing RBC (2nd RBC). The horizontal distance from the inlet boundary to the trailing RBC's center; l_1 is set to 3 μm and the distance between two RBCs' centers; l_2 is set to 5 μm. The

deformation index (*DI*) of the RBCs is calculated by *l*/*d* as **Eq (9)**, where *l* and *d* defined in the **Fig 4**.

$$DI = \frac{\text{Total length of the RBC}\,(l)}{\text{Total height of the RBC}\,(d)} \tag{9}$$

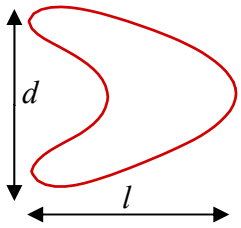

Fig 4: Deformed RBC; *DI* = *l*/*d*

When two cells move in the capillary, they start to deform from their initial biconcave shape to the parachute shape. However, the leading RBC exhibits a larger deformation compared to the trailing RBC (see **Fig 5** and **Fig 6**). The calculated *DI* of the leading RBC is even greater than that of the single RBC flowing through the same capillary under the same pressure gradient (see **Fig 5**). On the other hand, the trailing RBC shows a less deformation compared to the leading RBC and also its *DI* is less than that of the single RBC flowing alone in the same capillary (see **Fig 5**).

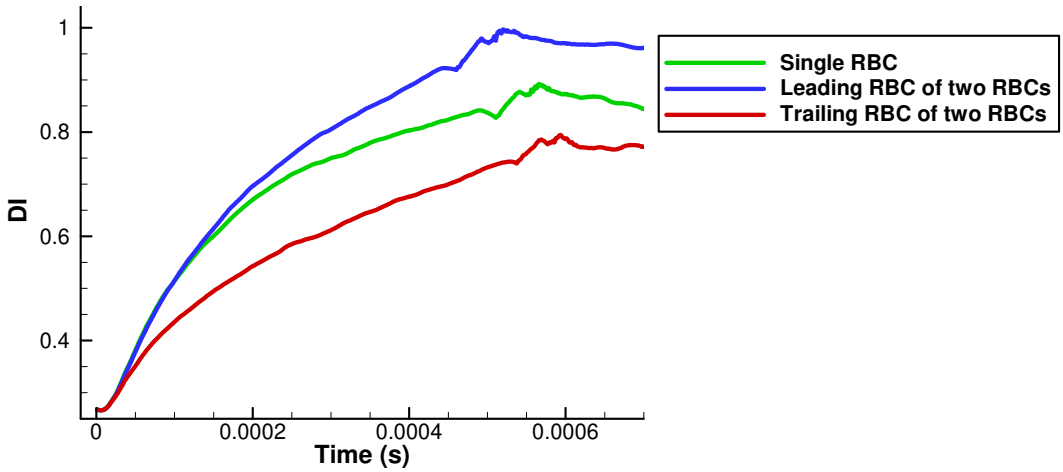

Fig 5: Variation of the *DI* of the RBCs with time; when two RBCs are present in an uniform capillary and a single RBC is present in the same capillary

This phenomenon occurs due to the hydrodynamic interaction between two RBCs (Pozrikidis 2005; Shi et al. 2013). It can be seen from **Fig 6** that the flow streamlines are disturbed due to the presence of two RBCs. The flow streamlines (in the *x*-direction) follow the capillary wall and are parallel to each other near the inlet boundary (see **Fig 6**) as a result of the applied pressure at the inlet of the capillary. However, when they reach the trailing RBC, the flow streamlines diverge from each other. According to the Bernoulli's principle the pressure behind the trailing RBC increases (see **Fig 7**), when the flow streamlines depart from each other. The departed flow streamlines flow almost parallel to each other again after the trailing RBC and they converge immediately after the leading RBC. The converged streamlines cause to create a low pressure region right after the leading RBC (see **Fig 7**). This pressure variation is not enormous to clearly demonstrate in a pressure field (see **Fig 7**). However, it causes to create a difference in the *DI* of two RBCs.

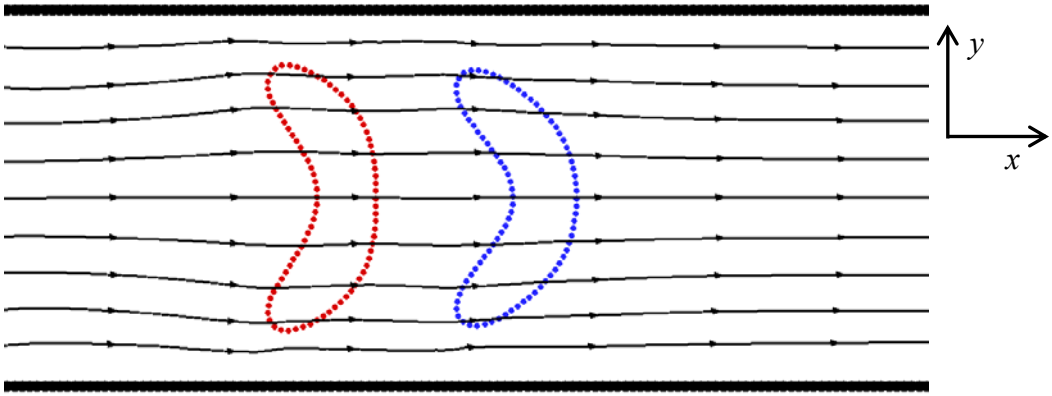

Fig 6: Velocity streamlines of the whole flow field, at $t = 0.080$ ms when two RBCs flow in a uniform capillary

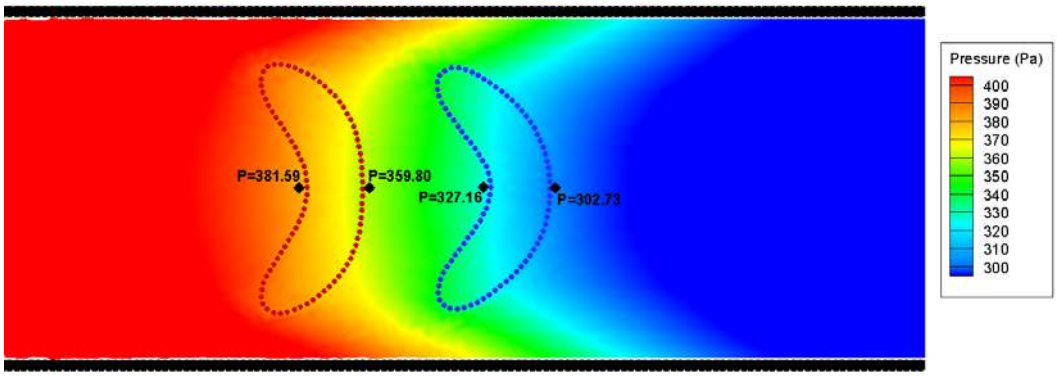

Fig 7: Pressure (P) variation of the flow field adjacent to two RBCs, at $t = 0.080$ ms when two RBCs flow in a uniform capillary

When the leading RBC flows in the *x*-direction (see **Fig 6**), it is not influenced by any other cell. Furthermore, as explained earlier, the pressure of the flow domain in the right-side of the leading RBC is lower compared to the left-side of the cell. Therefore, the leading RBC is subjected to a higher deformation. On the other hand, the leading RBC acts as an obstacle to the trailing RBC and the deformation of the trailing RBC is affected by the presence of the leading RBC. Furthermore, the trailing RBC seeks to drive the plasma particles between the trailing and leading RBCs and the pressure in the region between two RBCs rises. Therefore, an additional pressure is applied by the plasma particles on the left-side of the leading RBC. That pressure causes to deform the leading RBC further (see **Fig 5**). Meanwhile, the increased pressure in the flow region between two cells causes an additional pressure on the right-side of the trailing RBC. It results to reduce the deformation of the trailing RBC.

The mean velocities of two RBCs are slightly lower than that of a single RBC flows alone in the same capillary under the same pressure gradient (see **Fig 8**). Two RBCs act as an obstruction to the plasma flow and reduce the flow velocity of the whole flow field. As a result of this reduction of the flow velocity of the whole flow field the mean flow velocities of two RBCs are reduced. As can be seen in **Fig 8** the mean velocity of the leading RBC is slightly higher than that of the trailing RBC. Therefore, it can be predicted that the overall blood flow rate reduces slightly with the increased number of RBCs in the capillary due to the presence of more obstructions in the flow field.

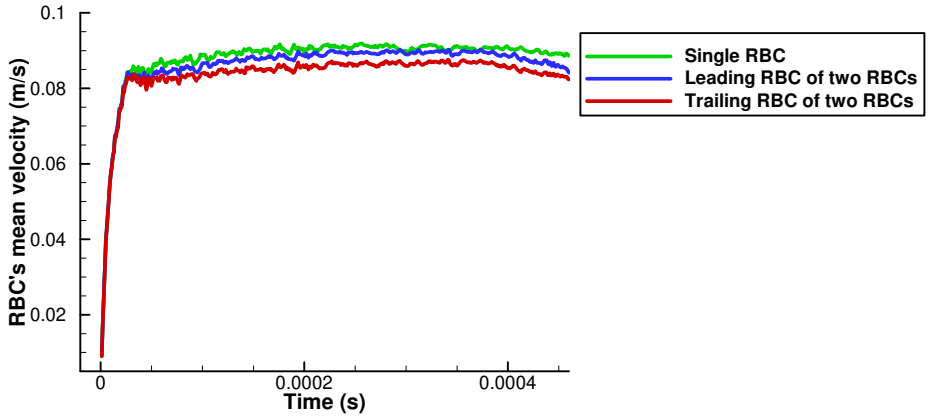

Fig 8: Variation of the mean velocity of the RBCs with time; when two RBCs are present in an uniform capillary and a single RBC is present in the same capillary

This slight variation of the velocities of the two RBCs happens to be due to the difference in the deformation of two RBCs. Since the deformation of the leading RBC is greater than that of the trailing RBC, the leading RBC follows the flow streamlines and makes fewer disturbances to the flow field. Therefore, the leading RBC's mean velocity is slightly higher than the mean velocity of the trailing RBC. It is clear that, the *DI* of a RBC depends on the number of RBCs in the capillary and the deformation of the RBCs varies even in the same capillary under the same pressure gradient. Even though the mean velocities of two RBCs show slight deviation, the amount of deformation of two RBCs are considerable. In the following sections the effects of the additional RBC in the capillary on the deformation of both RBCs are comprehensively studied.

3.2 Effect of the number of RBCs in the capillary

The effect of the number of RBCs on the deformation behavior of the RBCs is studied. The inlet pressure is set to 512.5 Pa, while the outlet pressure is set to zero. In this study, the number of RBCs in the capillary is changed from one to two and three. Here, l_1 is set to 3 μm and the distance between consecutive two RBCs is set to 5 μm.

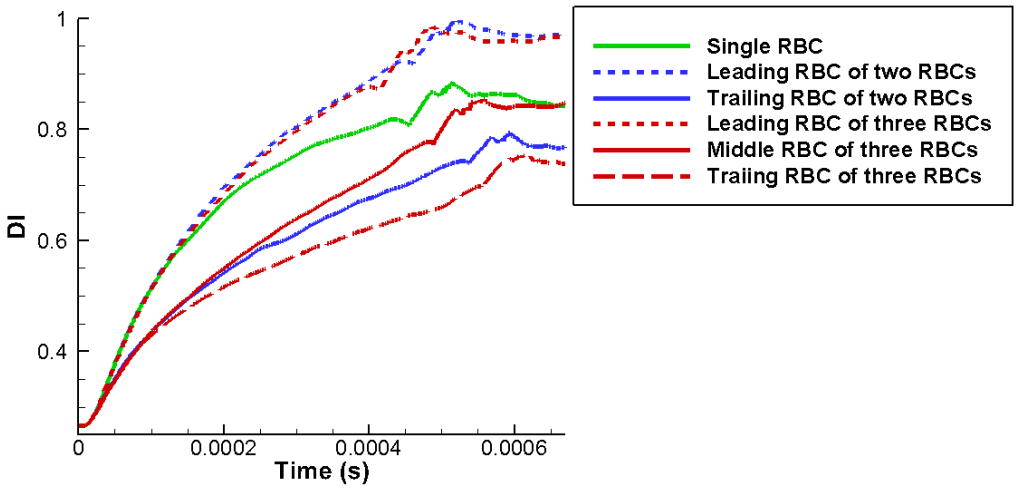

Fig 9: Variation of the *DI* of the RBCs with time, for different numbers of RBCs in the capillary

Simulation results reveal that when the number of RBCs in the capillary increases from one to two, the *DI* of the leading RBC increases and the *DI* of the trailing RBC decreases compared to the single RBC case (see **Fig 9**). Moreover, when the number of RBC increases to three the leading RBC shows a similar behavior as

the leading RBC in two RBCs case. However, the *DI* of the trailing RBC further reduces compared with that value of the trailing RBC of two RBCs case (see **Fig 9**). The middle RBC of three RBCs takes a in between value for the *DI* and it is very close to the *DI* of the single RBC condition (see **Fig 9**). Since blood continuously flows within the cardiovascular network, there is no leading or trailing RBC in the blood flow. Therefore, it can be concluded that all the RBCs would reach the same *DI* value, if there is a continuous flow of RBCs in a capillary.

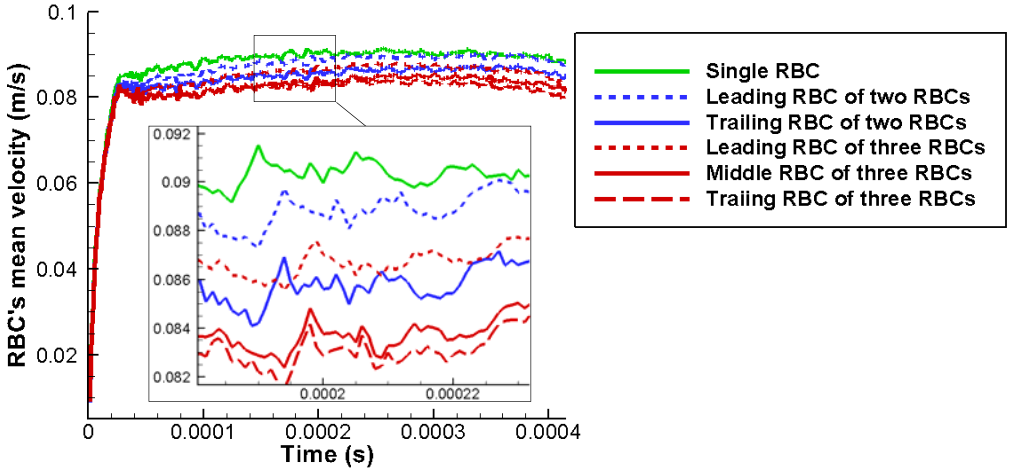

Fig 10: Variation of the mean velocity of the RBCs with time, for different numbers of RBCs in the capillary

Moreover, the mean velocity of the RBCs show slight variations from each other when the number of RBCs in the capillary changes. When there is only one RBC in the capillary, that RBC gains the highest mean velocity (see **Fig 10**). The mean velocity of the RBCs decreases when the number of RBCs in the capillary increases (see **Fig 10**). As can be seen in see **Fig 10**, the mean velocity of the trailing RBC of three RBCs is the lowest among all the RBCs' mean velocities.

In addition to that, the mean velocity of a RBC affects the *DI* of the RBC and it has been found that the deformation of the RBCs increases when the mean velocities of the RBCs increase (Shi et al. 2012). As can be seen in **Fig 9**, the *DI* of the leading RBC of three RBCs is slightly lower than that value of the leading RBC of two RBCs. This slight drop in the *DI* occurs due to the reduction in the mean velocity of the leading RBC of three RBCs compared to that value of the leading RBC of two RBCs.

In other words, when the number of RBCs in the capillary is increased it causes to decrease the mean velocities of the RBCs (see **Fig 10**). Generally, for a given capillary with a specific number of RBCs, the *DI* of the RBCs reduces when the mean velocities of the RBCs reduces. Therefore, it is not possible to compare the *DI*s of the RBCs even in the same capillary, when the number of RBCs changes. In order to clearly demonstrate the interactions between RBCs, only two RBCs are considered and thereby the effects of the changes in mean velocities of the RBCs (due to the change in number of RBCs) are eliminated.

3.3 Effect of the initial distance between two RBCs

The effect of the initial distance between two RBCs with similar properties on their deformation behavior is studied (see **Fig 11**). Here, l_1 is set to 3 μm and l_2 is varied to 3, 4, 5, 6 and 7 μm. When l_2 is equal or less than 2 μm, two RBCs are overlapped. Therefore, in this study, the minimum value used for l_2 is 3 μm. The inlet pressure is set to 512.5 Pa, while the outlet pressure is set to zero. The total length (L) and the diameter (D) of the capillary are set to 50 μm and 9.6 μm respectively. All the other simulation parameters are kept constant (see **Table 1**). The *DI* and mean velocities of two RBCs are analyzed for each case.

Simulation results reveal that when two RBCs are closer to each other at the beginning of the simulations (at $t = 0$), the difference between their *DI*s is higher when they reach the outlet of the capillary (see **Fig 11** and **Fig 12**). On the other hand, the *DI*s of the two cells do not show a considerable difference, when the initial distance between two RBCs is higher. As can be seen in **Fig 11 (a)** when the initial distance between two RBC is 3 μm, there is a noteworthy difference in the deformed shapes of two RBCs starting from $t = 0.08$ ms. The difference in the deformed shape increases with time and at $t = 0.40$ ms, it is very significant [see **Fig 11 (a)**]. However, when the initial distance between two RBC is 7 μm, there is no considerable difference in the deformed shapes of two RBCs [see **Fig 11 (e)**] at any time. The analysis of the pressure fields for each case suggest that the pressure difference (ΔP) between left and right hand sides of the trailing RBC increases with the initial distance between two RBCs (see **Fig 13**). Furthermore, it can be seen from **Fig 13** that the pressure difference for the leading RBC generally decreases when the initial distance between two RBCs increases.

Therefore, the pressure differences (ΔP) curves for leading and trailing RBCs approach to each other when the initial distance between two RBCs increases. As a result of that the two RBCs attain similar deformed shape, when the initial distance of two RBCs increases.

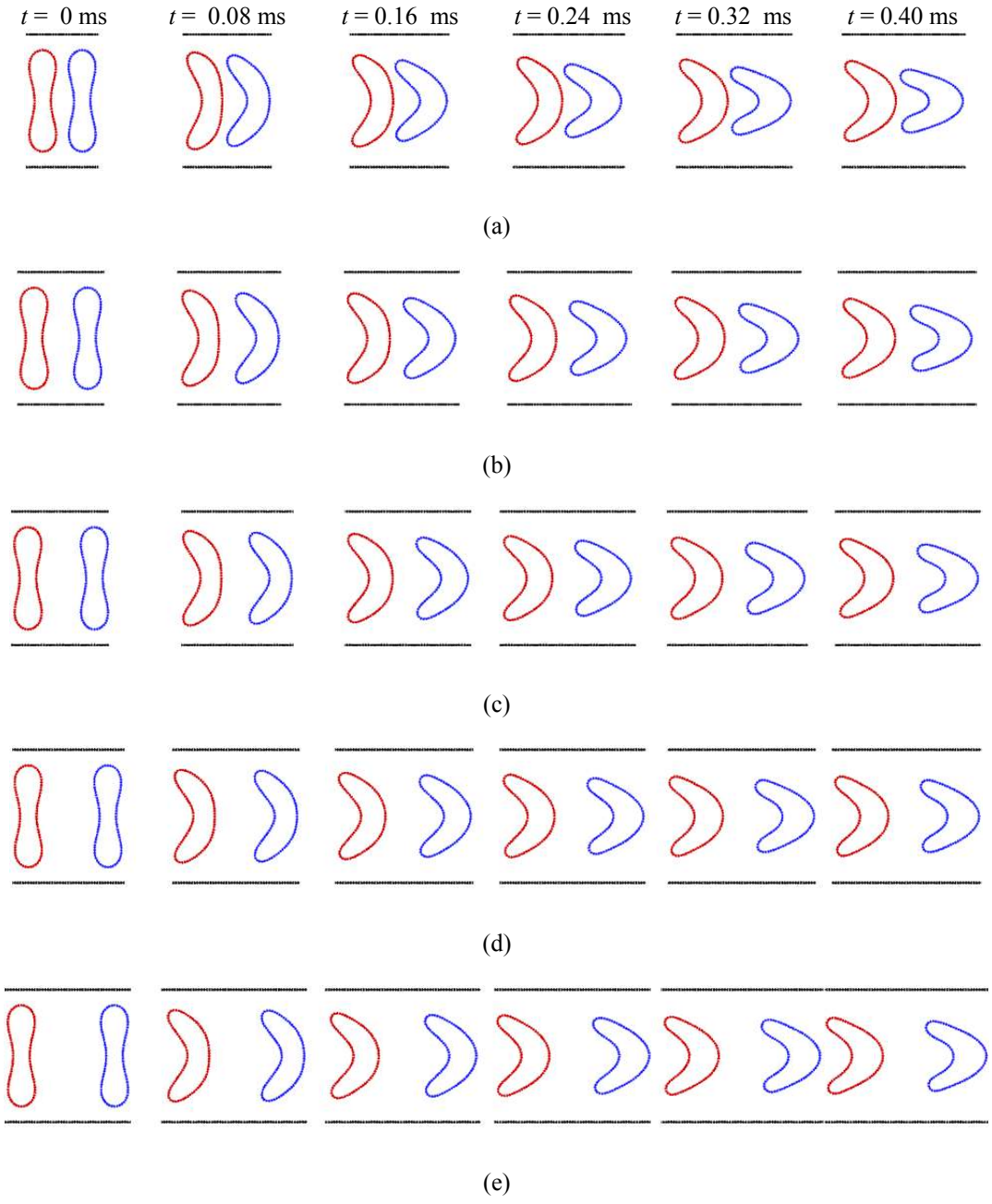

Fig 11: Deformed shapes of two RBCs at t = 0, 0.08, 0.16, 0.24, 0.32, and 0.40 ms, when the initial distance between two RBCs is (a) 3 μm, (b) 4 μm, (c) 5 μm, (d) 6 μm and (e) 7 μm; red-colour represents the trailing RBC and blue-colour represents the leading RBC

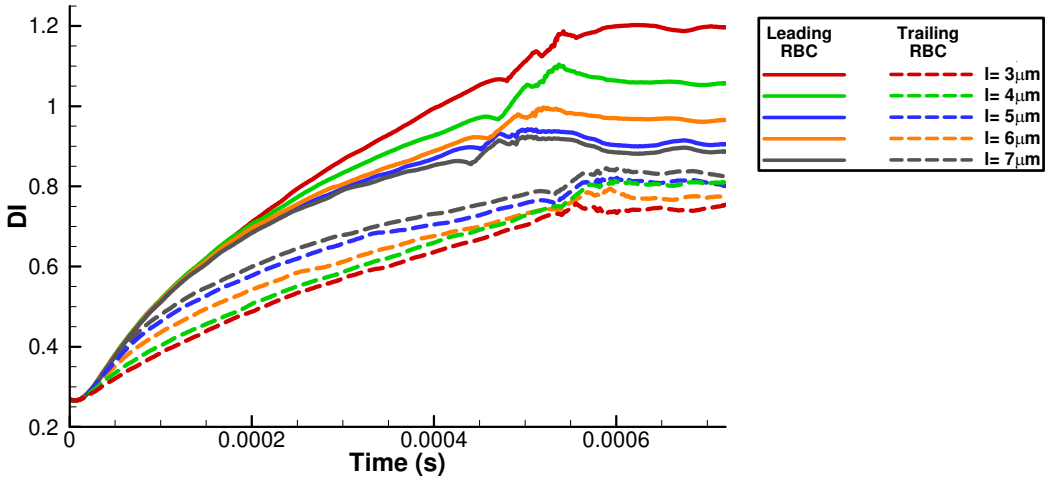

Fig 12: Variation of the *DI* of the leading and trailing RBCs with time; when the two RBCs are initially separated by a distance of *l*

Fig 12 shows the variation of the *DI* of two RBCs with time. The curves suggest that the RBCs' *DI* exhibit very little variation with time after about $t = 0.60$ ms. The leading RBC experiences the maximum deformation when the distance between two RBCs is 3 μm. On the other hand, the trailing RBC exhibits the minimum *DI* when the distance between two RBCs is 3 μm. The deformation of this RBC occurs slowly as the gradient of the curve is lesser, compared with the other curves in **Fig 12**.

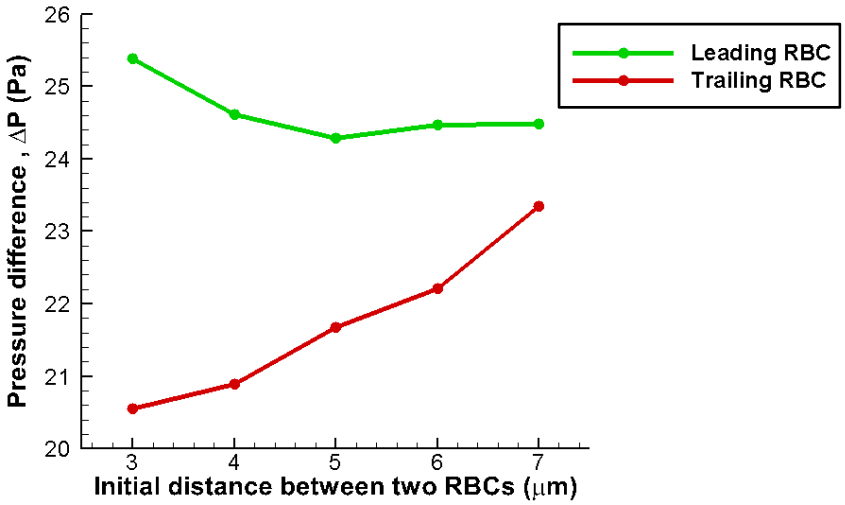

Fig 13: The variation of the pressure difference (ΔP) between left and right hand sided of two RBCs with initial distance between two RBCs at $t = 0.30$ ms

Although the deformed shapes of the leading RBC and trailing RBC are different from each other, the mean velocities of two RBCs do not show significant

deviation. However, there is a slight deviation of velocities of two RBCs. As can be seen in **Fig 14** the mean velocity of the leading RBC is slightly greater than that of the trailing RBC. Since the leading RBC's deformation is higher, compared with the trailing RBC, the leading RBC makes fewer disturbances to the flow stream lines and thus gains slightly higher mean velocity as explained earlier. Due to the difference in mean velocities of two RBCs, they depart from each other. The distance between two RBCs increases rapidly when the initial distance is 3 μm, and it reaches about 4.5 μm at $t = 0.4$ ms (see **Fig 15**). Conversely, the distance between two RBCs is increased by only 0.5 μm after 0.4 ms when the initial distance between two RBCs is 7 μm (see **Fig 15**). It can also be seen from **Fig 15** that the gradient of the curves decrease with the distance between two RBCs.

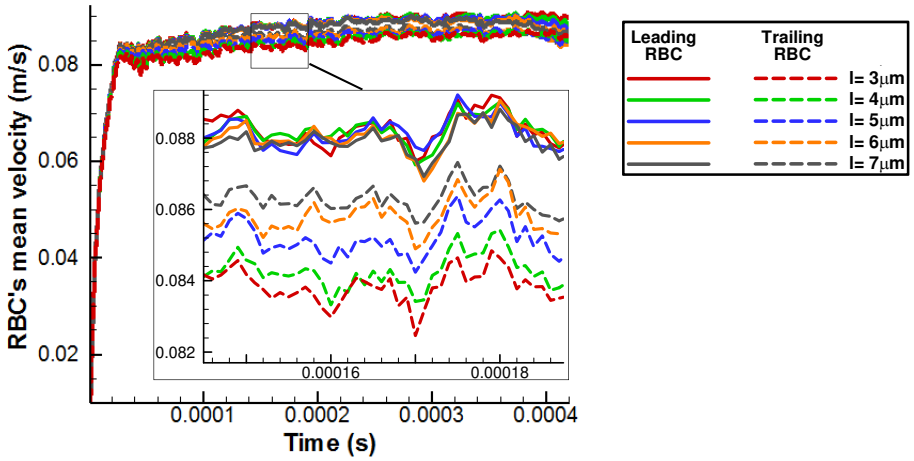

Fig 14: Variation of the mean velocity of the leading and trailing RBCs with time; for different initial distances (l) between two RBCs

In other words, when two RBCs are closer, the distance between two RBCs increases quickly (see **Fig 15**). As a result the hydrodynamic effect from one RBC on the other reduces. From **Fig 13**, it is evident that two RBCs in a given capillary tend to attain the same deformed shape when the distance between two RBCs increases, (due to the weakening of the hydrodynamic interaction between two RBCs).

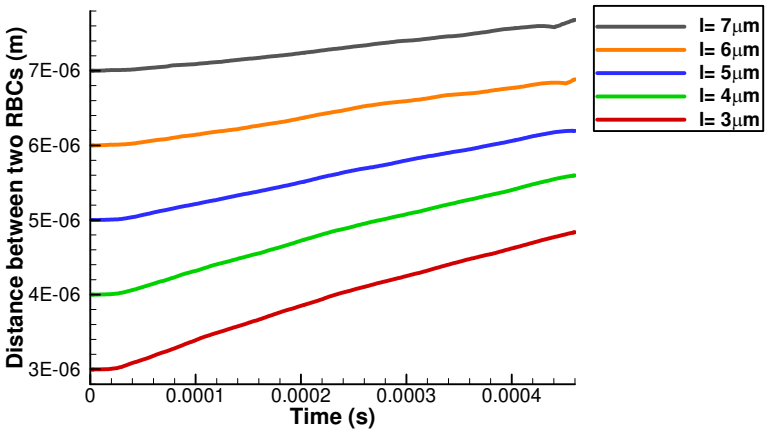

Fig 15: Variation of the distance between two RBCs with time; for different initial distances (l) between two RBCs

3.4 Effect of membrane bending stiffness

The effect of the membrane bending stiffness of one RBC on the deformation behavior of both RBCs is studied and presented in **Fig 16**. It has been found from the literature that the membrane deformability of the RBCs drop by more than ten times, compared with healthy RBCs, when RBCs are infected by a plasmodium parasite in malaria (Fedosov et al. 2011). Furthermore, it is found that the deformability of the cancer cells are higher than the healthy matured cells (Hou et al. 2009). In order to investigate the effects of an infected RBC on the deformation behavior of both RBCs, the membrane bending stiffness of one RBC is changed as described in the following sections. In the 1st study, the membrane bending stiffness of the leading RBC is changed from K_b to 0.01 K_b, 0.2 K_b, 10 K_b and 50 K_b while maintaining the membrane bending stiffness of the trailing RBC to K_b (5×10^{-10} Nm). Here, l_1 and l_2 are set to 3 μm and 5 μm respectively. The inlet pressure is set to 512.5 Pa, while the outlet pressure is set to zero. All the other simulation parameters are kept constant (see **Table 1**).

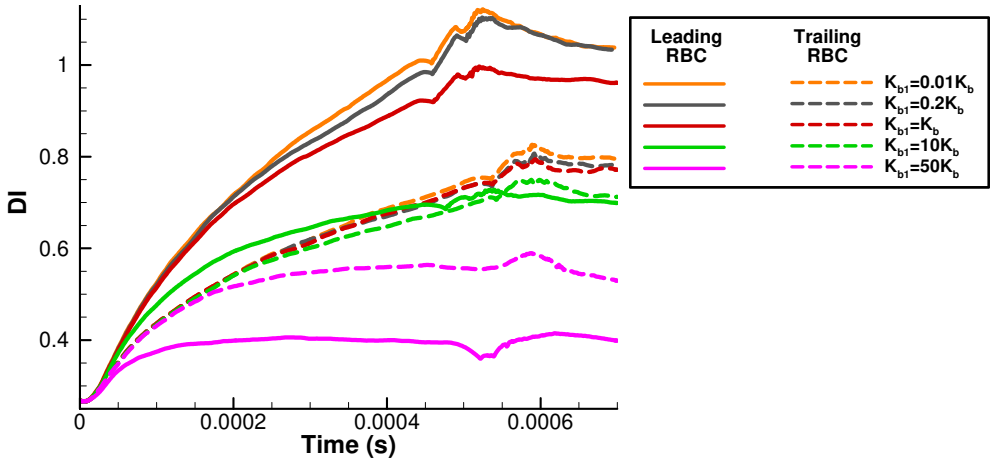

Fig 16: Variation of the *DI* of the leading and trailing RBCs with time; for different K_b values of the leading RBC with fixed K_b value of 5×10^{-10} Nm for the trailing RBC

It is clear that, if the membrane bending stiffness of a RBC increases, the *DI* of that RBC decreases. However, it can be seen that the changes in the membrane bending stiffness of the leading RBC affects the deformation of both RBCs (see **Fig 16**). When the membrane bending stiffness of the leading RBC is ten times greater than that of the trailing RBC, initially, the leading RBC deforms quickly (gradient of the curve is higher). However, after 0.50 ms both RBCs show almost the same deformed shape. The leading RBC with the membrane stiffness of 50 K_b shows the least bending deformation and its deformation occurs slowly (gradient of the curve is less). In this case the trailing RBC shows the second least deformation (see **Fig 16**) as its deformation is influenced by the leading RBC. On the other hand, the bending deformation of the leading RBC increases when the membrane bending stiffness of the leading RBC decreases to 0.2 K_b. However, the trailing RBC does not show any significant change in the deformed shape. Furthermore, when the leading RBC's membrane stiffness is decreased by hundred times, any considerable difference in the deformation of neither leading RBC nor trailing RBC is observed compared with the previous case (0.2 K_b).

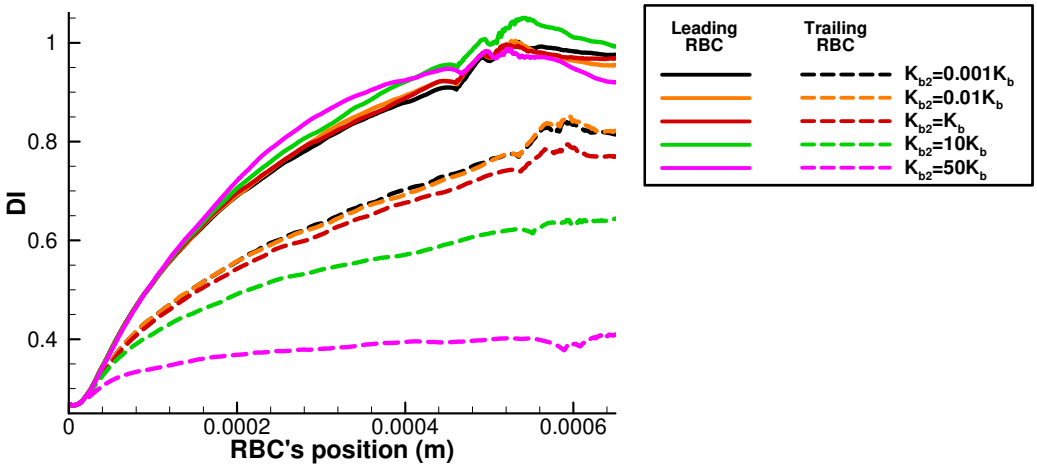

Fig 17: Variation of the *DI* of the leading and trailing RBCs with time; for different K_b values of the trailing RBC with fixed K_b value of 5×10^{-10} Nm for the leading RBC

In the 2nd study, the membrane bending stiffness of the trailing RBC is changed from K_b to 0.001 K_b, 0.01 K_b, 10 K_b and 50 K_b while maintaining the membrane bending stiffness of the leading RBC to K_b (5×10^{-10} Nm). All the other simulation parameters are kept constant (see **Table 1**). Simulation results reveal that, the deformation behavior of the leading RBC is not affected by the increase in the membrane bending stiffness of the trailing RBC (see **Fig 17**). Again, no significant variation in the deformation behavior of the leading RBC is observed when the membrane bending stiffness of the trailing RBC is reduced.

The mean velocities of both RBCs reduce when the membrane bending stiffness of the leading RBC increases (see **Fig 18**). However, the mean velocities of the RBCs do not show noticeable change with the decrease in the membrane bending stiffness in either leading RBC or trailing RBC (see **Fig 18** and **Fig 19**). On the other hand, the existence of the trailing RBC with higher membrane bending stiffness reduces the mean velocity of the leading RBC slightly, while the mean velocity of the trailing RBC reduces considerably (see **Fig 19**). Therefore, if the membrane stiffness of a RBC increases in the blood flow, it affects the mean velocities of other RBCs as well as the overall blood flow rate.

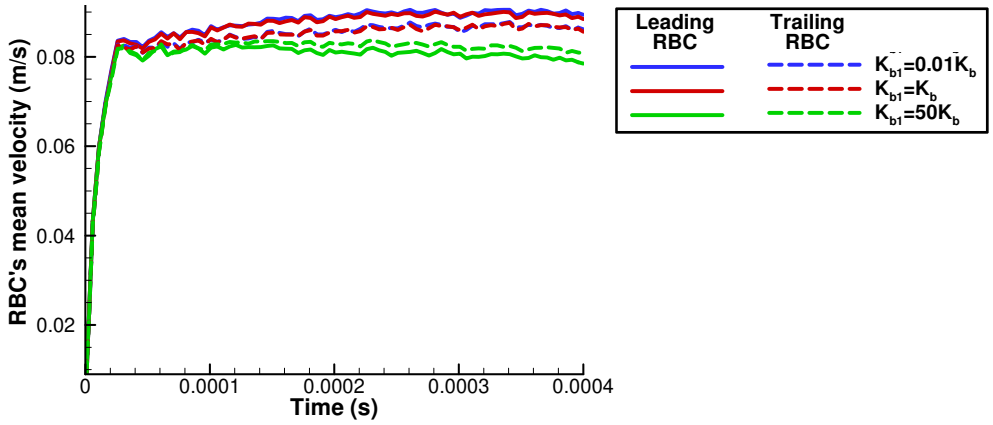

Fig 18: Variation of the mean velocity of the leading and trailing RBCs with time; for different K_b values of the leading RBC (K_{b1}) with fixed K_b value of 5×10^{-10} Nm for the trailing RBC

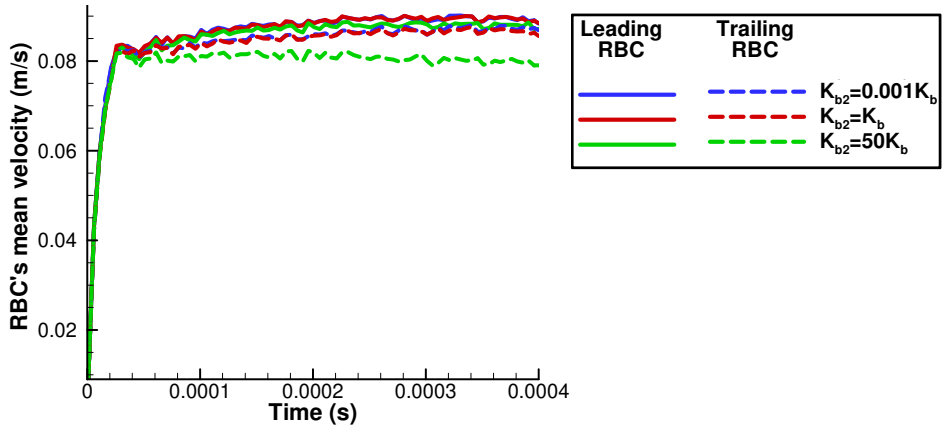

Fig 19: Variation of the mean velocity of the leading and trailing RBCs with time; for different K_b values of the trailing RBC (K_{b2}) with fixed K_b value of 5×10^{-10} Nm for the leading RBC

3.5 Effect of undeformed diameter of the RBC

In the above simulations the undeformed diameter of the RBC was set to 7.64 μm. However, it is an average value for a healthy RBC at rest. In general, the diameter of a healthy RBC varies between 6-8 μm (Dupire et al. 2012). In this study, the effect of the initial undeformed diameter of one RBC on the deformation behaviour of both RBCs is studied (see **Fig 20- Fig 24**). In order to change the initial undeformed diameter of the RBC, the radius of the initial circle (see **section 2**) is changed to 3.3 μm, 2.8 μm, 2.25 μm and 1.95 μm. Thereby the RBCs with initial diameters of 9.03 μm, 7.64 μm, 6.16 μm, and 5.29 μm are generated and are used for the following simulations. Although the diameter of healthy RBCs varies between 6-8 μm, RBCs with the diameters of 9.03 μm and 5.29 μm are

chosen for the simulations to clearly grasp the effect of the undeformed diameter of one RBC on the deformation behavior of both RBCs. In the 1st study, the initial undeformed diameter of the leading RBC is changed from 7.64 μm to 9.03 μm, 6.16 μm, and 5.29 μm while keeping the initial undeformed diameter of the trailing RBC to 7.64 μm. In this study, l_1 and l_2 are set to 3 μm and 5 μm respectively. The inlet pressure is set to 512.5 Pa, while the outlet pressure is set to zero. All the other simulation parameters are kept constant (see **Table 1**).

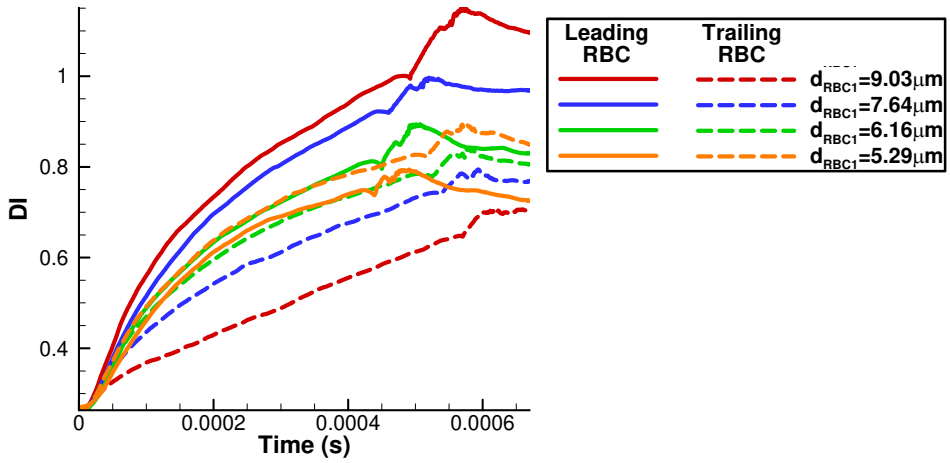

Fig 20: Variation of the *DI* of the leading and trailing RBCs with time; for different initial undeformed diameter values (d_{RBC1}) of leading RBC with fixed initial undeformed diameter of 7.64 μm for the trailing RBC

It can be seen from **Fig 20** that the change in the initial diameter of the leading RBC affects the *DI* of the tailing RBC. The increase of the initial diameter of the leading RBC causes to increase the *DI* of the leading RBC and it decreases the *DI* of the trailing RBC (see **Fig 20**). Since the leading RBC has a larger cross sectional area, it deforms more compared to the RBCs having smaller cross sectional areas and at the same time larger RBC disturbs the plasma flow more. As a result, the hydrodynamic interaction between two cells is greater and it directly affects the *DI*s of both RBCs (see **section 3.1**). Furthermore, the mean flow velocities of both RBCs reduce (see **Fig 21**) due to the existence of the larger leading RBC and it also affects the *DI* of the trailing RBC indirectly, which significantly reduces.

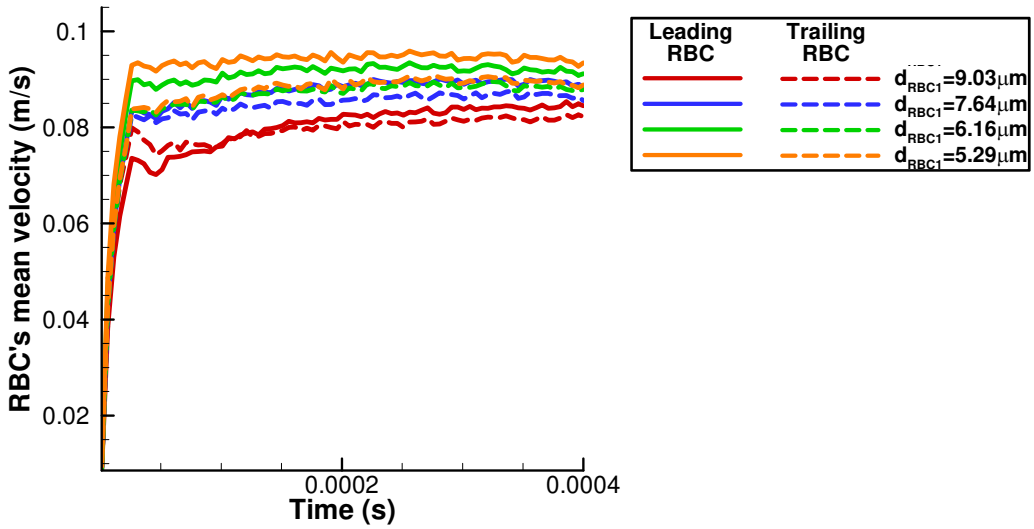

Fig 21: Variation of the mean velocity of the leading and trailing RBCs with time; for different initial undeformed diameter values (d_{RBC1}) of the leading RBC with fixed initial undeformed diameter of 7.64 μm for the trailing RBC

On the other hand, when the initial diameter of the leading RBC is 6.16 μm, due to the decrease in the initial undeformed diameter of the leading RBC, its *DI* reduces. Furthermore, less cross sectional area of the leading RBC makes fewer disturbances on the plasma flow and thereby the hydrodynamic interaction between two cells becomes weaker. Therefore, the two RBCs show almost similar *DI* whet $t = 0.0004$ s. Furthermore, when the initial diameter of the leading RBC is decreased to 5.29 μm, due to the further decrease in the initial undeformed diameter of the leading RBC, its *DI* further reduces. Thus, the cross sectional area of the leading RBC does not create a significant disturbance on the plasma flow and the hydrodynamic interaction between two cells becomes even weaker. Therefore, as explained in the **section 3.1**, the trailing RBC (which has the larger undeformed initial diameter) shows higher *DI*, while the leading RBC (which has the smaller undeformed initial diameter) shows lesser deformation.

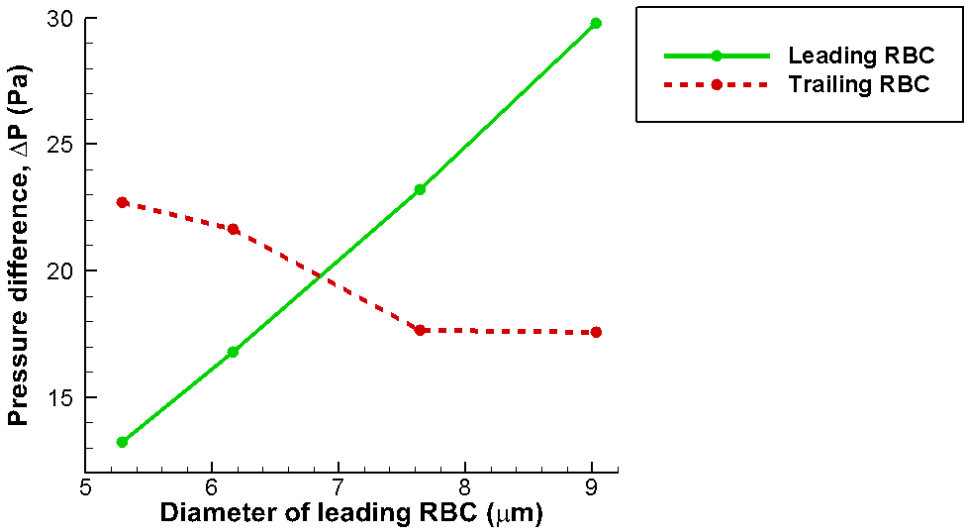

Fig 22: The variation of the pressure difference (ΔP) between left and right hand side of two RBCs with different initial undeformed diameter values of leading RBC (d_{RBC1}) at t = 0.20 ms

The analysis of the pressure fields for in this case suggest that the pressure difference (ΔP) between left and right had sides of the leading RBC increases with the initial undeformed diameter of the leading RBC (see **Fig 22**). Furthermore, it can be seen from **Fig 22** that the ΔP for the trailing RBC generally decreases when the initial undeformed diameter of the leading RBC increases. Therefore, as explained earlier, the RBCs experiencing higher ΔP exhibits larger *DI*s and the RBCs experiencing smaller ΔP exhibits lower *DI*s (**Fig 20**).

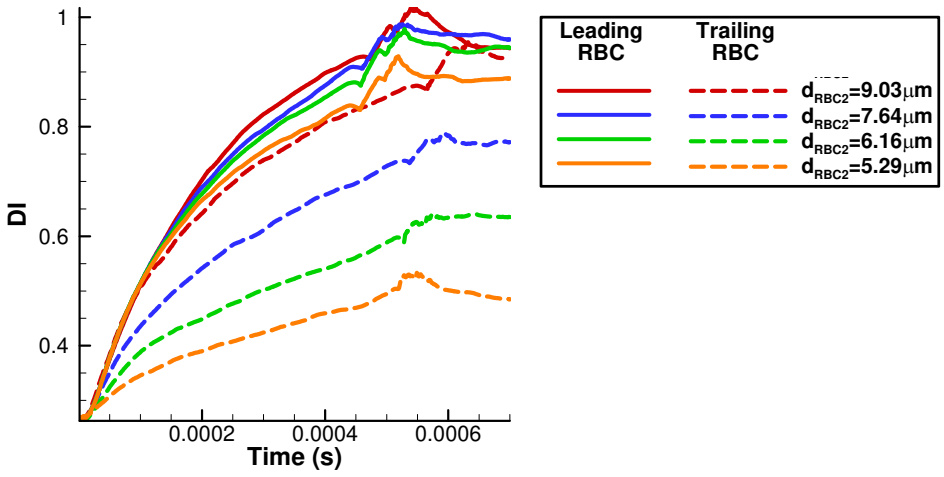

Fig 23: Variation of the *DI* of the leading and trailing RBCs with time; for different initial undeformed diameter values (d_{RBC2}) of the trailing RBC with fixed initial undeformed diameter of 7.64 μm for the leading RBC

In the 2nd study, the initial undeformed diameter of the trailing RBC is changed from 7.64 μm to 9.03 μm, 6.16 μm, and 5.29 μm while keeping the initial undeformed diameter of the leading RBC to 7.64 μm. Simulation results reveal that the deformation behavior of the leading RBC is not greatly affected by the increase in the initial undeformed diameter of the trailing RBC (see **Fig 23**). Moreover, there is no significant variation observed in the deformation behavior when the initial undeformed diameter of the trailing RBC is reduced. However, when the initial undeformed diameter of the trailing RBC is 5.29 μm, the *DI* of the leading RBC slightly reduces.

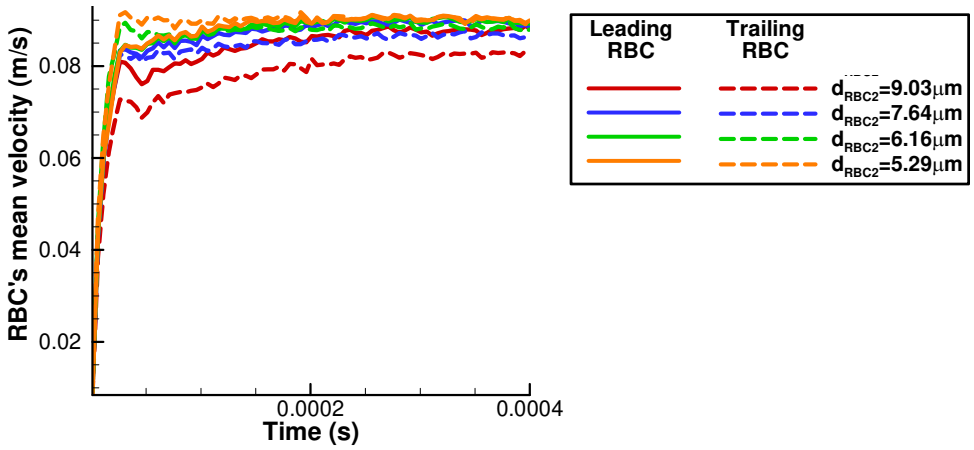

Fig 24: Variation of the mean velocity of the leading and trailing RBCs with time; for different initial undeformed diameter values (d_{RBC2}) of the trailing RBC with fixed initial undeformed diameter of 7.64 μm for the leading RBC

Whet $t = 0.0004$ s the mean velocity of the leading RBC is not significantly affected by the decrease in the initial undeformed diameter of the trailing RBC. However, it can be seen from **Fig 24** that the mean velocity of the trailing RBC reduces slightly, when the initial diameter of the trailing RBC is increased up to 9.03 μm. In this case, two RBCs take up a higher volumetric ratio in the problem domain due to the higher undeformed diameters (cross sectional area) of the trailing RBC. Therefore, compared with the other cases disturbance on the plasma flow is higher and as a result of it a slight drop in the mean velocities of the RBCs is expected.

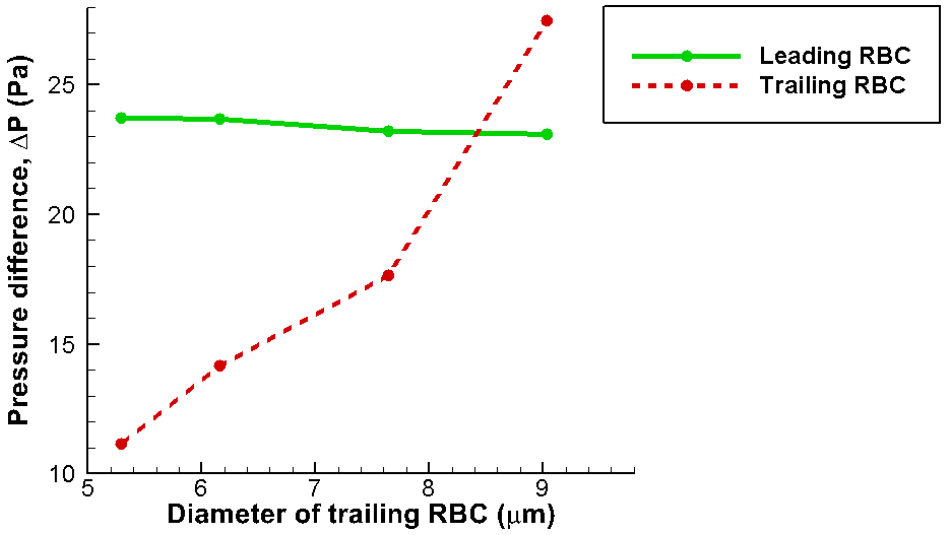

Fig 25: The variation of the pressure difference (ΔP) between left and right hand side of two RBCs with different initial undeformed diameter values of trailing RBC (d_{RBC2}) at t = 0.20 ms

Here, the analysis of pressure fields show that the pressure difference (ΔP) between left and right had sides of the leading RBC remains almost constant when the initial undeformed diameter of the trailing RBC increases (see **Fig 25**). Therefore, the leading RBCs do not show considerable variation of *DI* when the initial undeformed diameter of the trailing RBC increases (see **Fig 23**). However, it can be seen from **Fig 25** that the ΔP for the trailing RBC increases when the initial undeformed diameter of the trailing RBC increases. As can be seen from **Fig 23** and **Fig 25** the *DI*s of the trailing RBCs change according to the ΔP

3.6 Deformation of two RBCs in a stenosed capillary

There is a high risk of microvascular blockage in the blood vessels with stenosed section (Cooke et al. 2001). In order to predict the behavior of the RBCs through these sections, the motion and deformation of two RBCs in a stenosed capillary is studied and presented in this section. The behavior of two RBCs in the stenosed capillary is compared with the behavior of a single RBC in the same capillary. The total length (L) and the diameter (D) of the capillary are set to 60 μm and 9.6 μm respectively, while the minimum diameter of the stenosed area (d) is set to 5.6 μm. The inlet pressure is set to 615 Pa, while the outlet pressure is set to zero. The horizontal distance from the inlet boundary to the trailing RBC's center; l_1 is set to 3 μm and the distance between two RBCs' centers; l_2 is set to 5 μm. In order to compare the behavior of two RBCs, under the same simulation conditions a

single RBC is used with $l_1 = 8\ \mu$m [case 1; see **Fig 26** (b)] and $l_1 = 3\ \mu$m [case 2; see **Fig 26** (c)] to individually simulate the behavior of the leading and trailing RBCs respectively.

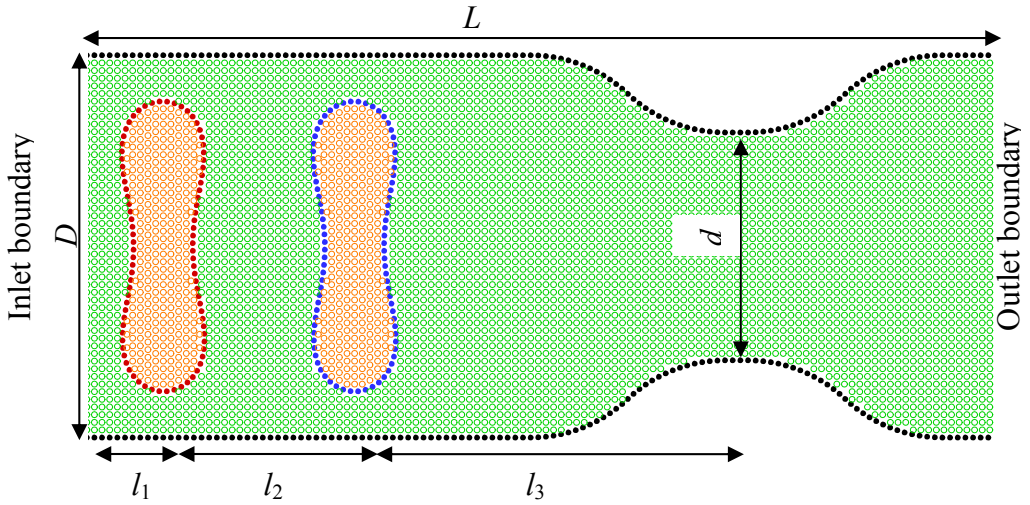

(a)

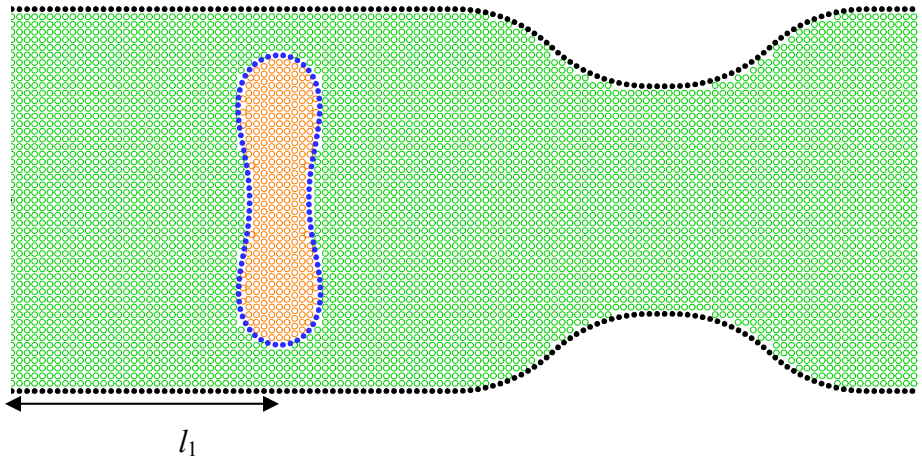

(b) case 1

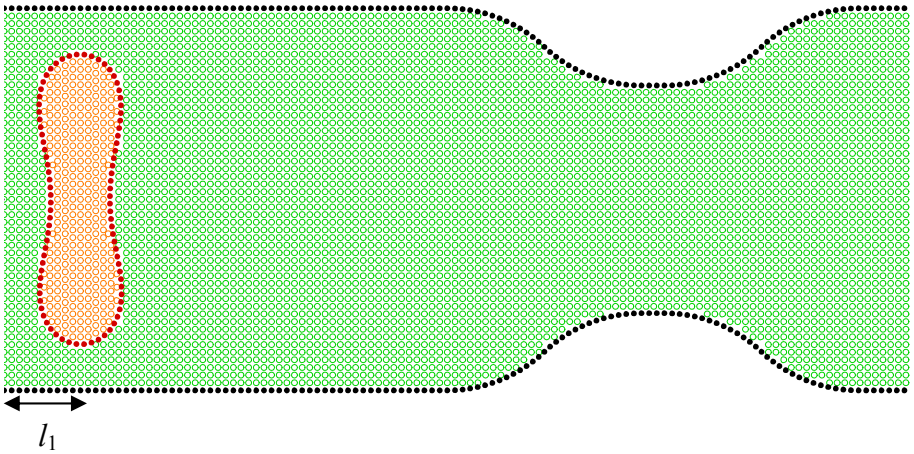

(c) case 2

Fig 26: Initial particle configuration of the flow filed when (a) Two RBCs in the stenosed capillary, (b) Case 1: A single RBC in the stenosed capillary with l_1 = 8 μm (c) Case 2: A single RBC in the stenosed capillary with l_1 = 3 μm

Similar to the previous simulations due to the applied pressure at the inlet, plasma particles and RBCs start to move. The leading RBC of two RBCs shows a higher *DI* compared to that of the trailing RBC when it moves through the narrowest section in the capillary (see **Fig 27**). The results in **Fig 27** reveal that the *DI* of the leading RBC of two RBCs is even greater than that of the single RBC in case 1 [where l_1 = 8 μm; **Fig 26 (b)**]. Furthermore, the *DI* of the trailing RBC is less than that of the single RBC in the case 2 [where l_1 = 3 μm; **Fig 26 (c)**]. This increase in the *DI* of the leading RBC and decrease in the *DI* of the trailing RBC of two RBCs occur due to the hydrodynamic interactions between two RBCs compared with the single RBC cases [**Fig 26 (b)** and **(c)**] This simulation results further reveal that, when there is a single RBC in the stenosed capillary, the maximum *DI* of the RBC increases, as the initial distance of the RBC from the narrowest section of the capillary increases (see **Fig 27**).

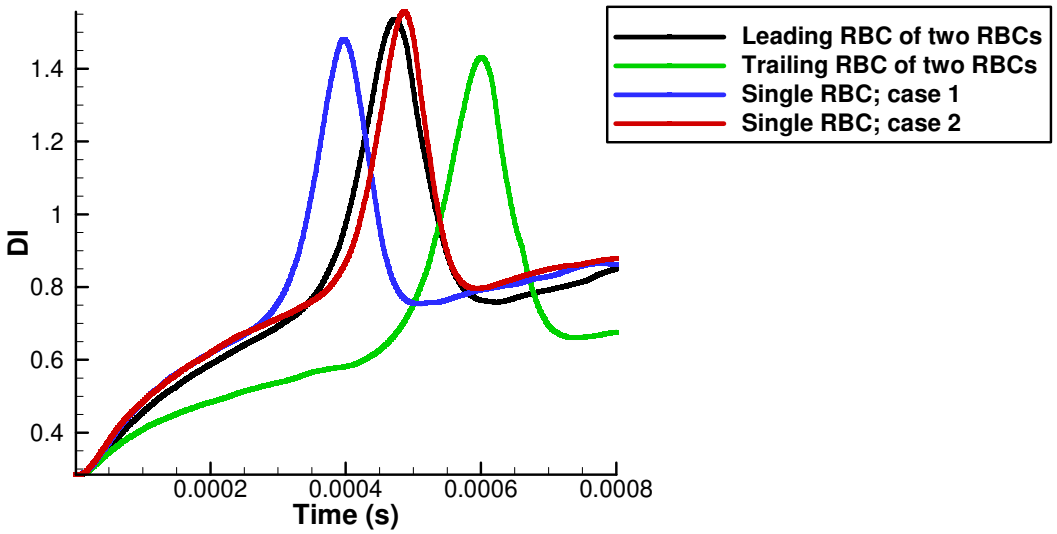

Fig 27: Variation of the *DI* of the RBCs with time; when two RBCs are present in a stenosed capillary and a single RBC is present in the same capillary at different positions

Interestingly, as shown in **Fig 28** the mean velocities of two RBCs are noticeably lower than the single RBC situations [case 1; **Fig 26** (b) and case 2; **Fig 26** (c)]. Therefore, two RBCs take longer time to reach the stenosed section of the capillary and the outlet of the flow domain. It can be seen from **Fig 28** that

initially two RBCs move almost at the same mean velocity. Since the blood flow rate is constant in a capillary for a given pressure, flow velocity increases, when the flow area reduces in the stenosed section. Similarly, when the leading RBC is moving through the stenosed section of the capillary its mean velocity increases significantly. During this time period the leading RBC slightly blocks the plasma flow through the stenosed section in the capillary and as a result of it a small reduction of the trailing RBC's mean velocity can be seen (see **Fig 28**).The trailing RBC also reaches its maximum mean velocity when it passes though the stenosed section. However, at that time no noticeable change in the mean velocity of the leading RBC can be observed, since the leading RBC is already downstream of the capillary. Finally, when both RBCs exit from the stenosed section the mean velocities of the RBCs increase and they reach a similar velocity with a very slight reduction compared to that of the single RBC cases case 1; **Fig 26** (b) and case 2; **Fig 26** (c)].

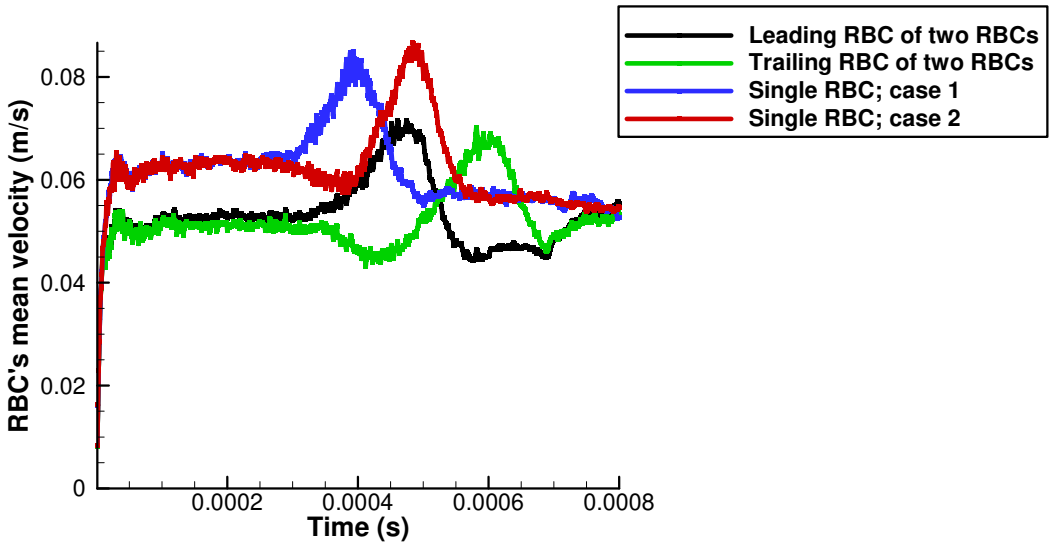

Fig 28: Variation of the mean velocity of the RBCs with time; when two RBCs are present in a stenosed capillary and a single RBC is present in the same capillary at different positions

4. Conclusions

A two-dimensional spring network model based on the DEM concepts is successfully used in combination with the SPH method to study the interaction between two RBCs and its effect on their motion and deformation. From this study, the below conclusions may be drawn.

- Due to the hydrodynamic interaction between two RBCs, the leading RBC is always subjected to a higher deformation compared to the trailing RBC. The leading RBC's *DI* is greater than that of a single RBC flows in the same capillary under the same conditions. The trailing RBC's *DI* is less than that of a single RBC flows in the same capillary under the same conditions.
- The distance between two RBCs makes a significant impact on the motion and deformation of two RBCs. When two RBCs are moving closer to each other, the hydrodynamic interaction between two RBCs is higher and the relative velocity of two RBCs is also higher, which cause to increase the distance between two RBCs.
- When the leading RBC becomes stiffer as a result of infection by a disease like malaria, it directly affects the motion and deformation of the trailing RBC. However, the motion and deformation of the leading RBC is not greatly influenced by the properties of the trailing RBC.
- RBCs with larger undeformed diameters slow down the mean velocity of the RBCs as well as the blood flow rate.
- When the capillary has a stenosed section the mean velocity of both RBCs decrease significantly before the stenosed section. However, after the stenosed section they gain their velocity back similar to the uniform capillary situation.

Furthermore, it is expected to extend the study to three dimensional RBCs, to capture more realistic motions and deformations of the RBCs.

Acknowledgements

Support provided by the ARC Future Fellowship grant (FT100100172), ARC Discovery grant (DP150100828) and the High Performance Computer (HPC) resources in Queensland University of Technology (QUT) are gratefully acknowledged. The fourth author acknowledge that the Australian Governments fully fund the Australian Red Cross Blood Service for the provision of blood products and services to the Australian community

References

Bayliss, L.: The axial drift of the red cells when blood flows in a narrow tube. The Journal of physiology **149**(3), 593-613 (1959). doi:http://dx.doi.org/10.1113/jphysiol.1959.sp006363

Cooke, B.M., Mohandas, N., Coppel, R.L.: The malaria-infected red blood cell: structural and functional changes. Advances in parasitology **50**, 1-86 (2001). doi:http://dx.doi.org/10.1016/S0065-308X(01)50029-9

Dupire, J., Socol, M., Viallat, A.: Full dynamics of a red blood cell in shear flow. Proceedings of the National Academy of Sciences **109**(51), 20808-20813 (2012). doi:http://dx.doi.org/10.1073/pnas.1210236109

Fåhræus, R., Lindqvist, T.: The viscosity of the blood in narrow capillary tubes. American Journal of Physiology--Legacy Content **96**(3), 562-568 (1931). doi:http://ajplegacy.physiology.org/content/96/3/562

Fedosov, D.A., Lei, H., Caswell, B., Suresh, S., Karniadakis, G.E.: Multiscale modeling of red blood cell mechanics and blood flow in malaria. PLoS computational biology **7**(12), e1002270 (2011). doi:http://dx.doi.org/10.1371/journal.pcbi.1002270

Frcitas, R.A.: Exploratory design in medical nanotechnology: a mechanical artificial red cell. Artificial Cells, Blood Substitutes and Biotechnology **26**(4), 411-430 (1998). doi:http://dx.doi.org/10.3109/10731199809117682

Hou, H.W., Li, Q., Lee, G., Kumar, A., Ong, C., Lim, C.T.: Deformability study of breast cancer cells using microfluidics. Biomedical microdevices **11**(3), 557-564 (2009). doi:http://dx.doi.org/10.1007/s10544-008-9262-8

Jiang, X.M., Wang, T., Xing, Z.W.: Simulation Study of Hemodynamics of Red Blood Cells in Stenotic Microvessels. Advanced Materials Research **647**, 321-324 (2013). doi:http://dx.doi.org/10.4028/www.scientific.net/AMR.647.321

Kaoui, B., Harting, J., Misbah, C.: Two-dimensional vesicle dynamics under shear flow: Effect of confinement. Physical Review E **83**(6), 066319 (2011). doi:http://dx.doi.org/10.1103/PhysRevE.83.066319

Le, D.-V., White, J., Peraire, J., Lim, K., Khoo, B.: An implicit immersed boundary method for three-dimensional fluid–membrane interactions. Journal of computational physics **228**(22), 8427-8445 (2009). doi:http://dx.doi.org/doi:10.1016/j.jcp.2009.08.018

Liu, G.R., Liu, M.: Smoothed particle hydrodynamics: a meshfree particle method. World Scientific Publishing Company Incorporated, (2003)

Morris, J.P., Fox, P.J., Zhu, Y.: Modeling low Reynolds number incompressible flows using SPH. Journal of computational physics **136**(1), 214-226 (1997). doi:http://dx.doi.org/doi:10.1006/jcph.1997.5776

Nagayama, K., Honda, K.: 3D Particle Simulations of Deformation of Red Blood Cells in Micro-Capillary Vessel. (2012)

Pan, T.W., Wang, T.: Dynamical simulation of red blood cell rheology in microvessels. International Journal of Numerical Analysis & Modeling **6**, 455-473 (2009). doi:http://www.math.ualberta.ca/ijnam/Volume-6-2009/No-3-09/2009-03-07.pdf

Polwaththe-Gallage, H.-N., Saha, S.C., Sauret, E., Flower, R., Gu, Y.: Numerical Investigation of Motion and Deformation of a Single Red Blood Cell in a Stenosed Capillary. International Journal of Computational Methods, 1540003 (2015)

Polwaththe-Gallage, H.N., Gu, Y., Saha, S.C., Senadeera, W., Oloyede, A.: Numerical simulation of red blood cells' motion : a review. Paper presented at the 4th International Conference on Computational Methods (ICCM 2012), Crowne Plaza, Gold Coast, QLD,

Polwaththe-Gallage, H.N., Saha, S.C., Gu, Y.: Deformation of a single red blood cell in a microvessel. ANZIAM Journal **55**, C64--C79 (2014). doi:http://journal.austms.org.au/ojs/index.php/ANZIAMJ/article/view/7828

Pozrikidis, C.: Axisymmetric motion of a file of red blood cells through capillaries. Physics of Fluids (1994-present) **17**(3), 031503 (2005). doi:http://dx.doi.org/10.1063/1.1830484

Pries, A., Secomb, T., Gaehtgens, P.: Biophysical aspects of blood flow in the microvasculature. Cardiovascular research **32**(4), 654-667 (1996). doi:http://dx.doi.org/10.1016/S0008-6363(96)00065-X

Secomb, T.: Flow-dependent rheological properties of blood in capillaries. Microvascular Research **34**(1), 46-58 (1987)

Shi, L., Pan, T.W., Glowinski, R.: Deformation of a single red blood cell in bounded Poiseuille flows. Physical Review E **85**(1), 016307 (2012). doi:http://dx.doi.org/10.1103/PhysRevE.85.016307

Shi, X., Lin, G., Zou, J., Fedosov, D.A.: A lattice Boltzmann fictitious domain method for modeling red blood cell deformation and multiple-cell hydrodynamic interactions in flow. International Journal for Numerical Methods in Fluids **72**(8), 895-911 (2013). doi:http://dx.doi.org/10.1002/fld.3764

Shvartsman, L.D., Fine, I.: Optical transmission of blood: effect of erythrocyte aggregation. Biomedical Engineering, IEEE Transactions on **50**(8), 1026-1033 (2003). doi:http://dx.doi.org/10.1109/TBME.2003.814532

Sun, C., Munn, L.L.: Particulate nature of blood determines macroscopic rheology: a 2-D lattice Boltzmann analysis. Biophysical journal **88**(3), 1635-1645 (2005). doi:http://dx.doi.org/10.1529/biophysj.104.051151

Suresh, S., Spatz, J., Mills, J.P., Micoulet, A., Dao, M., Lim, C.T., Beil, M., Seufferlein, T.: Connections between single-cell biomechanics and human disease states: gastrointestinal cancer and malaria. Acta Biomaterialia **1**(1), 15-30 (2005). doi:http://dx.doi.org/10.1016/j.actbio.2004.09.001

Tsubota, K.-i., Wada, S., Yamaguchi, T.: Simulation study on effects of hematocrit on blood flow properties using particle method. Journal of Biomechanical Science and Engineering **1**(1), 159-170 (2006). doi:http://doi.org/10.1299/jbse.1.159

Ye, T., Phan-Thien, N., Khoo, B.C., Lim, C.T.: Dissipative particle dynamics simulations of deformation and aggregation of healthy and diseased red blood cells in a tube flow. Physics of Fluids (1994-present) **26**(11), 111902 (2014). doi:http://dx.doi.org/10.1063/1.4900952